

Estimating the number of available states for normal and tumor tissues in gene expression space

Frank Quintela (1,2) and Augusto Gonzalez (3,2)

(1) University of Modena, Italy

(2) Institute of Cybernetics, Mathematics and Physics,
Havana, Cuba

(3) University of Electronic Science and Technology,
Chengdu, People Republic of China

March 3, 2022

Abstract

Gene expression data for a set of 12 localizations from The Cancer Genome Atlas are processed in order to evaluate an entropy-like magnitude allowing the characterization of tumors and comparison with the corresponding normal tissues. The comparison indicates that the number of available states in gene expression space is much greater for tumors than for normal tissues and points out to a scaling relation between the fraction of available states and the overlapping between the tumor and normal sample clouds.

1 Introduction

The extreme difficulties in treating cancer [1] reveal that the survival capabilities of cancer cells are much stronger than those of the somatic cells in our body. restricted by the conditions of homeostasis. The reason for such “advantages” is explained in the atavistic theory of cancer [2, 3, 4, 5, 6] as

the result of a core genetic programme, which helped primitive multicellular organisms to overcome the extreme conditions posed by the ancient earth.

One aspect of these enhanced capabilities is related to tissue fitness. Cancer cells are known to turn off the mechanism of fitness control in homeostasis and exhibit replication rates much higher than the stem cells in healthy tissues [7].

In vivo measurements of fitness in normal and tumor tissues is a difficult task. However, there is a way of looking at fitness which is related to the number of available states for a system in configuration space and may be the subject of numerical computations. Indeed, for a tissue (or a small portion of it) there should be a fitness landscape in gene expression space. Regions of high fitness are characterized by their volumes which, in some sense, measure the number of available states for the system.

In the present paper, we aim at estimating the number of available states for normal and tumor tissues or, more precisely, the ratio of numbers for the tumor and the corresponding normal tissue. To this end, we process gene expression data for 12 cancer localizations, coming from The Cancer Genome Atlas (TCGA) portal [8], and introduce an entropy-like magnitude measuring the volume or the number of available states in gene expression space.

The main result is that, as expected, the number of available states for tumors are much higher than for normal tissues. An homeostatic tissue has much less possibilities of realization or much higher order than the primitive multicellular tumor. Additional facts are discussed below.

2 Results and Discussion

2.1 Entropy in gene expression space

As mentioned, our starting point is the TCGA expression data for 12 tumors and the corresponding normal tissues. The selected localizations are characterized by more than 20 normal and more than 300 tumor samples, as shown in Table 1.

We perform a Principal Component Analysis [9, 10, 11] of the expression data. Methodological aspects are briefly explained in the Methods section below. In paper [12], we study the topology of gene expression space for normal and tumor tissues. We sketch the main results of that paper that

Table 1: The set of studied cancer localizations and the main results of the paper. TCGA abbreviations are used.

Tissues	Normal samples	Tumor samples	ΔS	S_{tumor}	$-\ln I$
BRCA	112	1096	17.92	89.16	62.10
COAD	41	473	29.93	90.87	87.50
HNSC	44	502	12.67	89.48	58.02
KIRC	72	539	22.22	89.31	68.16
KIRP	32	289	29.86	90.40	82.34
LIHC	50	374	29.00	90.16	63.94
LUAD	59	535	26.24	92.18	66.08
LUSC	49	502	28.59	90.58	75.25
PRAD	52	499	9.79	85.96	49.85
STAD	32	375	19.82	93.10	64.17
THCA	58	510	15.00	85.62	54.51
UCEC	23	552	26.06	93.26	77.78

shall be used in our computations:

1. Although there are around 60000 genes, normal tissues and tumors span a region with reduced effective dimension.

Then, we will use the first 20 principal components in order to describe the state of a sample in gene expression space (GES). These 20 components capture no less than 85 % of the total variance in the dispersion of experimental samples in GES.

2. For a given tissue, normal samples are well separated from tumor samples in GES. Both regions seem to be the basins of attraction of two singular points: the normal homeostatic and the cancer attractors.

Fig. 1 upper panel shows as example the (PC1, PC2) plane for Lung Squamous Cell cancer (LUSC in TCGA notations). Points in the figure represent samples from different patients. The clouds of points are grouped in well defined regions defining the attractors. We shall estimate the volume of each region, which gives an indication of the number of accessible states.

More precisely, for both normal tissues and tumors we shall introduce the entropy-like magnitude:

$$S = - \int d^D \underline{x} \rho(\underline{x}) \ln \rho(\underline{x}), \quad (1)$$

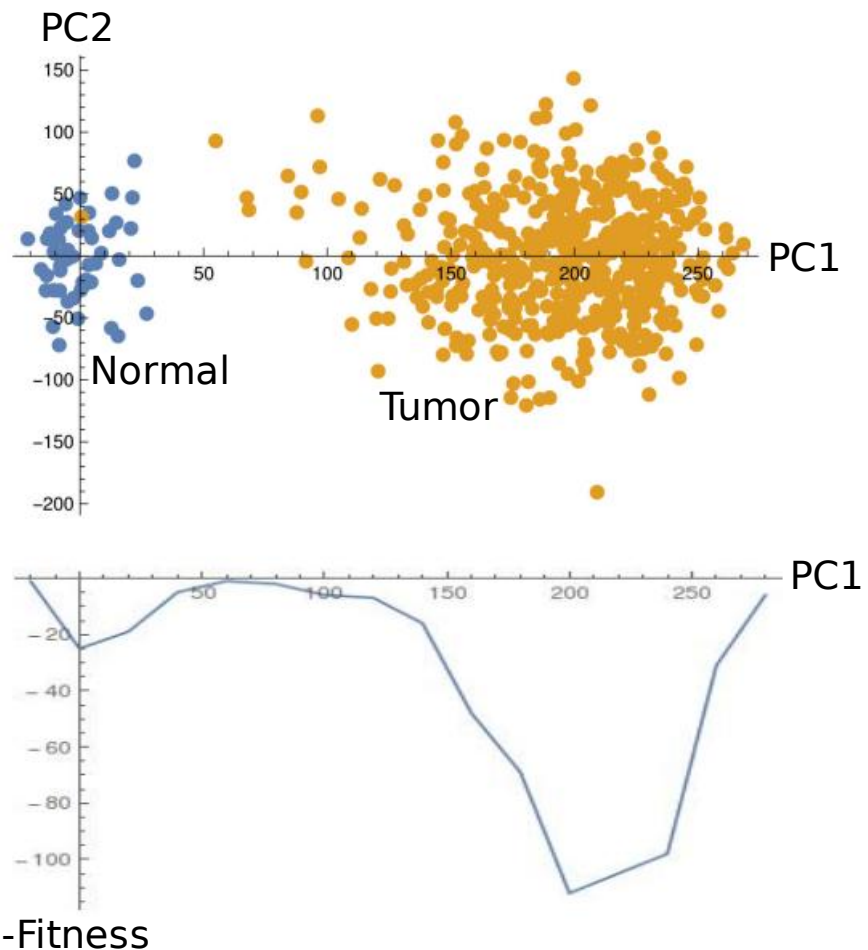


Figure 1: Upper panel: PCA of gene expression data for Squamous Cell Lung cancer (LUSC). The first axis (PC1) discriminates between a normal sample and a tumor. Lower panel: Schematics of the fitness landscape.

where $D = 20$ is the number of principal components to be used in the description of the system in GES, and ρ is the probability density, coming from a fit to the observed sample data.

The relation between the S magnitude and the volume of the basin of attraction is roughly $S \approx \ln(Vol)$, thus S measures the logarithm of the number of available states in the region.

We fit the observed distribution of sample points to a multivariate gaussian density, ρ . This procedure guarantees a maximal entropy. Details are found in the Methods chapter below.

We show in Table 1 the magnitudes S_{tumor} and $\Delta S = S_{tumor} - S_{normal}$ for the set of tissues under study. The number of states in GES seems to be much larger for tumors than for normal tissues, leading to $\Delta S \gg 1$.

On the other hand, the number of accesible states appears to be nearly constant for all tumors. Normal tissues exhibit larger variations, which could be related to tissue differentiation. In other words, the process of de-differentiation of tumors [13] involves the increase of the accesible volume in GES to a nearly constant value.

2.2 Configurational “complexity map”

In the analysis of complex systems, it is usual to add a second magnitude, besides entropy, and construct a complexity map [14]. In our problem, we have already estimated the volumes of the basins of attraction. We may introduce an additional magnitude characterizing the transition region between the two attractors. In this way, we may compare the different tumors or, more precisely, tumor-normal tissue pairs according to their configurations in GES.

Let us define the density overlap:

$$I = \int d^D \underline{x} \sqrt{\rho_{tumor}(\underline{x}) \rho_{normal}(\underline{x})}. \quad (2)$$

The magnitude I measures the overlapping between the clouds of normal and tumor samples. The square root is introduced for normalization purposes. Analytic expressions for I when ρ are gaussian distributions are provided in the Methods chapter below.

Table 1 and Fig. 2 show that the number of accesible states is very similar for all tumors, but shows higher variation in normal tissues. If we

take this number as an indication of “structure”, one may think that the colon (COAD) is more structured than the prostate (PRAD).

With regard to the observed overlap between tumor and normal clouds of points, a first aspect to be stressed is the distance between the centers of the clouds. In PRAD, THCA and HNSC the centers are much closer than in COAD, KIRP and UCEC.

From the overlap one may also infer properties of the fitness landscape. Indeed, one may assume that the observed density of samples at a given point of GES is somehow proportional to the fitness. In Fig. 1 lower panel we schematically represent the fitness distribution in LUSC. The curve is obtained simply from the histogram of samples. Notice that in the intermediate region there are practically no samples. The curve is highly peaked at the attractor points, and very shallow in the intermediate region. In PRAD, THCA and HNSC, on the other hand, there are many more samples in the intermediate region, meaning that the fitness is higher in this region. Samples in the intermediate region are related in paper [12] to tumors in the initial stages of progression.

The numbers in Table 1 and Fig. 1 indicate also the apparent correlation between $-\ln I$ and ΔS , i.e. $-\ln I = 1.36 \Delta S + 37.07$ or $I \sim (Vol_n/Vol_t)^{1.36}$. The nature of this dependence is intriguing. The fact is that the larger the entropy difference (the ratio of basin volumes) the smaller the overlapping between the tumor and normal sample clouds. We do not have an interpretation for this fact.

2.3 Fitness landscape and transition rates

The normal homeostatic state shall be protected against transitions to the cancer state by a barrier. Otherwise the transitions are unavoidable because both the fitness and the number of available states in the cancer region are much higher than in the normal region.

It is natural to assume that the intermediate region holds a low-fitness barrier, as schematically represented in Fig. 1 lower panel for Lung Squamous Cell Cancer (LUSC). Indeed, the normal homeostatic state is a state with regulated fitness [15]. In cancer, on the other hand, these constraints are removed and tumor growth is only limited by the availability of space and nutrients. The intermediate region is a space for senescence or different kinds of illness, where fitness is reduced and the compensation mechanisms are not capable of keeping homeostasis. In paper [12] it was shown that tumors in

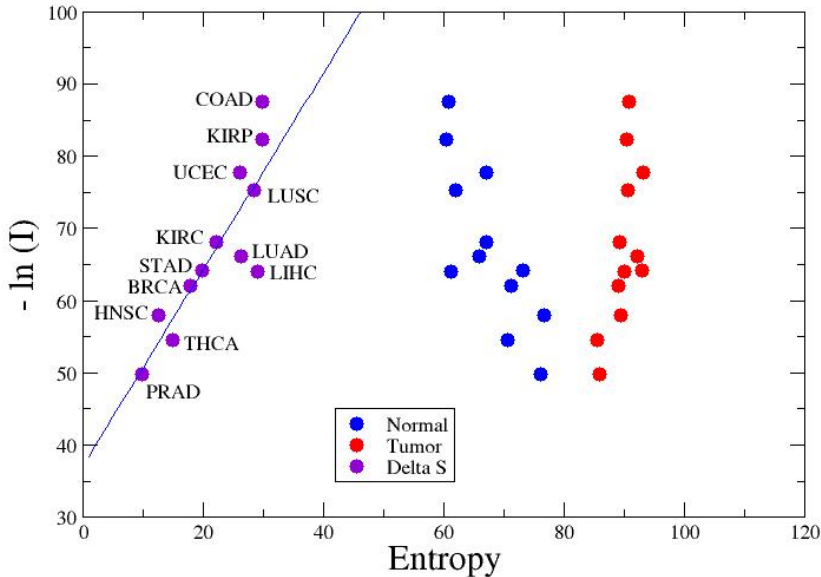


Figure 2: The entropy-overlapping map. Notice that tumors exhibit a nearly constant entropy, and that there is an exponential relationship between the overlap I and the entropy variation ΔS .

the initial stages of progression transit through this region.

In Fig. 1 lower panel the x axis, as in the upper panel, is PC1, which was identified as the cancer axis [12] separating the normal from the cancer states. The y axis is the fitness (with a minus sign). The absolute maximum of fitness is cancer. The normal homeostatic state is a local metastable maximum, which should be characterized by a mean decay time, τ_H .

Notice that with a rough estimation of the fitness landscape along the PC1 axis we could get, in principle, an estimation for τ_H , and thus the risk of cancer in a tissue.

The time for the reverse process to occur, τ_C , that is from the tumor to the normal state, is expected to be much larger than τ_H . We could get a rough value for it by using a detailed balance equation [16]:

$$\tau_c = \tau_H \frac{N_{states}(C)}{N_{states}(H)} = \tau_H \exp(\Delta S). \quad (3)$$

Taking $\tau_H \approx 60$ years we get for prostate tumors, for example, $\tau_c \approx 10^6$ years. For thyroid cancer, on the other hand, $\tau_c \approx 2 \times 10^8$ years.

These are fictitious numbers, not related to any biological processes. We compute them with the only purpose of confirming that the progression to cancer is an almost irreversible process.

However, it is a curious fact that the required times for early multicellular organisms to evolve to modern metazoans are precisely hundreds of My [17]. At the level of conglomerates of cells one can imagine evolution as jumps against entropy, that is from states like C to states like H. These are highly improbable processes which, however, may be the source of further advantages. When one says that it may take 200 My to occur, it means that from the many conglomerates living in this time period a few of them could make the transition and start a new line of evolution.

2.4 Concluding remarks

We estimated the volumes of the basins of attraction in gene expression space for the normal and cancer regions in each of the 12 cancer localizations described in Table 1. These volumes, which are proportional to the number of accessible micro-states, are measured by means of a “configurational” entropy-like magnitude, constructed from the probability density of samples in the space. The latter is obtained from a multivariate gaussian fit to the observed distribution of samples.

The results are mainly three: 1. The number of accessible states is much higher for tumors than for normal samples, 2. All studied tumor localizations have roughly the same number of accessible states, and 3. The overlap between the tumor and normal samples clouds of points is roughly proportional to $\exp(-\Delta S)$.

The reduced number of accessible states for the normal tissue can be interpreted as a higher level of organization than the tumor. The higher variability of entropy in normal tissues, on the other hand, can be taken as a manifestation of tissue differentiation and structure. However, the biological relevance of the scaling between cloud overlapping and the entropy difference should be further clarified.

3 Methods

The TCGA data of Table 1 is analyzed by means of the PCA technique. The details of the PC analysis are described in paper [12]. Me briefly sketch them in the present section.

Gene expression are given in FPKM format. The number of genes is 60483. This is the dimension of matrices in the Principal Component analysis. Usually, in order to compute the average expression of a gene the median or the geometric mean are used. We prefer geometric averages, but then the data should be slightly distorted to avoid zeroes. To this end, we added a constant 0.1 to the data. By applying this regularization procedure, genes identified as relevant could be under question if the differential expression is relatively low and their expression in normal tissues is near zero. As we are mainly interested in the strongly over- or under-expressed genes, they are out of the question.

We take the mean geometric average over normal samples in order to define the reference expression for each gene, e_{ref} . Then the normalized or differential expression is defined as: $e_{diff} = e/e_{ref}$. The fold variation is defined in terms of the logarithm $\hat{e} = \log_2(e_{diff})$. Besides reducing the variance, the logarithm allows treating over- and sub-expression in a symmetrical way.

Deviations and variances are measured with respect to $\hat{e} = 0$. That is, with respect to the average over normal samples. This election is quite natural, because normal samples are the majority in a population.

With these assumptions, the covariance matrix is written:

$$\sigma_{ij} = \sum \hat{e}_i(s)\hat{e}_j(s)/(N_{samples} - 1), \quad (4)$$

where the sum runs over the samples, s , and $N_{samples}$ is the total number of samples (normal plus tumor). $\hat{e}_i(s)$ is the fold variation of gene i in sample s .

As mentioned, the dimension of matrix is 60483. By diagonalizing it, we get the axes of maximal variance: the Principal Components (PCs). They are sorted in descending order of their contribution to the variance.

In LUSC, for example, PC1 accounts for 67% of the variance. This large number is partly due to our choice of the reference, $\hat{e} = 0$, and the fact that most of the samples are tumors. The reward is that PC1 may be defined as the cancer axis. The projection over PC1 defines whether a sample is classified as normal or tumor.

The next PCs account for a smaller fraction of the variance. PC2 is responsible of 4%, PC3 of 3%, etc. Around 20 PCs are enough for an approximate description of the region of the gene expression space occupied by the set of samples.

We want to compute only a small number of the eigenvalues and eigenvectors of σ . To this end, we use a Lanczos routine in Python language, and run it in a node with 2 processors, 12 cores and 64 GB of RAM memory. As a result, we get the first 100 eigenvalues and their corresponding eigenvectors.

For a sample, the projections over the PC vectors define the new coordinates. These are the starting data for the computation of the configurational entropy. We organize it as 24 matrices M , each one corresponding to a tissue in a stage, i.e. $M(LIHC, tumor)$. The number of columns in any case is 20 (number of Principal Components) and the number of rows is the number of samples, as reported in Table 1.

From M the sample covariance matrix, Σ , is defined as

$$\Sigma_{jk} = \frac{1}{N-1} \sum_{i=1}^N (M_{ij} - \mu_j)(M_{ik} - \mu_k), \quad (5)$$

where $\mu_j = \frac{1}{N} \sum_{i=1}^N M_{ij}$ is the mean value of coordinate j in the set of samples.

In order to find probability distributions for the sets of normal and tumor samples we maximize the entropy taking the covariance matrices as constraints. These are quadratic constraints, thus the result is a multivariate gaussian [18]:

$$\rho(\underline{x}) = \frac{1}{(2\pi)^{\frac{D}{2}} \sqrt{|\Sigma|}} \exp\left\{-\frac{1}{2}(\underline{x} - \underline{\mu})^T \Sigma^{-1} (\underline{x} - \underline{\mu})\right\}. \quad (6)$$

Notice our convention for vectors, \underline{x} . There are advantages in using this procedure. First, with normal distributions we may analytically compute the quantities of interest, second this distribution is, in accordance with the Central Limit Theorem, an estimation of the actual distribution for much larger data sets, and third this distribution is, from the point of view of information theory, the most unbiased one with regard to data covariance, that is no heuristic criteria have been used for choosing it.

For our target quantities, the entropy and the overlap integral, we get:

$$S = \frac{1}{2} \ln |\Sigma| + \frac{D}{2}(1 + \ln 2\pi), \quad (7)$$

$$I = 2^{\frac{D}{2}} \frac{|\Lambda_n|^{1/4} |\Lambda_t|^{1/4}}{|\Lambda_c|^{1/2}} \exp\{(\eta_c^T \Lambda_c^{-1} \eta_c - \mu_n^T \Lambda_n \mu_n - \mu_t^T \Lambda_t \mu_t)/4\}, \quad (8)$$

where $\Lambda_j = \Sigma_j^{-1}$ for $j = n, t$; $\eta_c = \Lambda_n \mu_n + \Lambda_t \mu_t$, and $\Lambda_c = \Lambda_n + \Lambda_t$.

Acknowledgements A.G. acknowledges the Cuban Program for Basic Sciences, the Office of External Activities of the Abdus Salam Centre for Theoretical Physics, and the University of Electronic Science and Technology of China for support. The research is carried on under a project of the Platform for Bio-informatics of BioCubaFarma, Cuba. The data for the present analysis come from the TCGA Research Network [8].

References

- [1] Victoria da Silva-Diz, Laura Lorenzo-Sanz, Adri Bernat-Peguera, et al (2018). Cancer cell plasticity: Impact on tumor progression and therapy response. *Semin. Cancer Biol.* 53: 48-58.
- [2] P.C.W. Davies and C. H. Lineweaver (2011). Cancer tumors as Metazoa 1.0: tapping genes of ancient ancestors. *Phys. Biol.* 8(1): 015001.
- [3] Tomislav Domazet-Loo and Diethard Tautz (2010). Phylostratigraphic tracking of cancer genes suggests a link to the emergence of multicellularity in metazoa. *BMC Biology* 8: 66.
- [4] Charles H. Lineweaver, Paul C. W. Davies and Mark D. Vincent (2014). Targeting cancers weaknesses (not its strengths): Therapeutic strategies suggested by the atavistic model. *Bioessays* 36: 827835.
- [5] Luis Cisneros, Kimberly J. Bussey, Adam J. Orr, et al (2017). Ancient genes establish stress-induced mutation as a hallmark of cancer. *PLoS ONE* 12(4): e0176258.
- [6] Anna S Trigos, Richard B Pearson, Anthony T Papenfuss, and David L Goode (2019). Somatic mutations in early metazoan genes disrupt regulatory links between unicellular and multicellular genes in cancer. *ELife* 8: e40947.

- [7] Alberts, B., Bray, D., Hopkin, et al (2013). Essential cell biology. Garland Science.
- [8] The TCGA Research Network: <https://www.cancer.gov/tcga>.
- [9] Svante Wold, Kim Esbensen, and Paul Geladi (1987). Principal component analysis. *Chemometrics and intelligent laboratory systems* 2(1-3): 37-52.
- [10] Jake Lever, Martin Krzywinski and Naomi Altman (2017). Principal component analysis. *NATURE METHODS* 14: 641-642.
- [11] Markus Ringnr (2008). What is principal component analysis?. *NATURE BIOTECHNOLOGY* 26: 303-304.
- [12] Augusto Gonzalez, Yasser Perera and Rolando Perez. On the gene expression landscape of cancer. arXiv:2003.07828.
- [13] FriedmannMorvinski, D., and Verma, I. M. (2014). Dedifferentiation and reprogramming: origins of cancer stem cells. *EMBO reports*, 15(3), 244-253.
- [14] Feldman, D. P., McTague, C. S., and Crutchfield, J. P. (2008). The organization of intrinsic computation: Complexity-entropy diagrams and the diversity of natural information processing. *Chaos: An Interdisciplinary Journal of Nonlinear Science*, 18(4): 043106.
- [15] Benoit Biteau,Christine E. Hochmuth, and Heinrich Jasper (2011). Maintaining Tissue Homeostasis: Dynamic Control of Somatic Stem Cell Activity. *Cell Stem Cell* 9: 402-411.
- [16] Jin Wang (2014). Landscape and flux theory of non-equilibrium dynamical systems with application to biology. *Advances in Physics* 64: 1-137.
- [17] Andrew H. Knoll and Martin A. Nowak (2017). The timetable of evolution. *Sci. Adv.* 3: e1603076.
- [18] A. Caticha (2012). Entropic inference and the foundations of physics. Brazilian Chapter of the International Society for Bayesian Analysis- ISBrA, Sao Paulo, Brazil.